JOURNAL OF Applied Polymer SCIENCE

Nanoparticles based on β-conglycinin and chitosan: Self-assembly, characterization, and drug delivery

Yong Liu,[1] Jieyi Liang,[1] Shoulian Wei,[1] Ling Liu,[1] Miaochan Liao[2]

[1]School of Chemistry and Chemical Engineering, Zhaoqing University, Zhaoqing, People's Republic of China

[2]Department of Logistics Management, Zhaoqing University, Zhaoqing, People's Republic of China

Yong Liu contributed to the writing of the article, the research design, and the analysis of the drug-release mechanism. Jieyi Liang contributed to the turbidity measurements. Shoulian Wei contributed to the acquisition and analysis of the Fourier transform infrared data. Ling Liu contributed to the acquisition and analysis of the scanning electron microscopy and dynamic light scattering data. Miaochan Liao contributed to the acquisition of the drug-release data. All of the authors approved the submitted and final versions of this article.

Correspondence to: Y. Liu (E-mail: lygdut@163.com)

ABSTRACT: The purpose of this study was to fabricate and evaluate nanoparticles based on β-conglycinin (7S) and chitosan (CS) to deliver 5-fluorouracil (5-FU). The nanoparticles were prepared with a self-assembly method. Turbidity measurements performed at 600 nm were used to investigate the formation of the nanoparticles as a function of the pH, 7S-to-CS mass ratio, and total concentration of 7S and CS. The optimum conditions for the preparation of the nanoparticles were a pH of 5.5, a 7S-to-CS mass ratio of 4 : 1, and total concentration of 7S and CS of 9 mg/mL. Under these conditions, the nanoparticles in solution had a high turbidity and good stability. Fourier transform infrared spectroscopy revealed that the nanoparticles were formed mainly through electrostatic interactions between the amine groups ($-NH_3^+$) of CS and the carboxyl groups ($-COO^-$) of 7S. Scanning electron microscopy micrographs and dynamic light scattering analysis showed that the nanoparticles had an approximately spherical morphology with a smooth surface, and the mean particle size was about 120 nm with a narrow size distribution. The release of 5-FU showed an initial burst release followed by a sustained release, and the release was pH-dependent. The release mechanism of 5-FU was Fickian diffusion according to the Ritger–Peppas model. © 2015 Wiley Periodicals, Inc. J. Appl. Polym. Sci. **2015**, *132*, 41963.

KEYWORDS: drug delivery systems; nanoparticles; nanowires and nanocrystals; self-assembly

Received 13 September 2014; accepted 5 January 2015

DOI: 10.1002/app.41963

INTRODUCTION

Nanotechnology is widely used in the pharmaceutical and medicine industries for drug delivery, disease detection, biosensors,[1] and so on. Nanoparticles for drug delivery have particular advantages because they not only protect the drugs but also facilitate the drugs to go across critical and specific biological barriers and hit specific targets.[2] Also, nanoparticles can increase the stability, bioactivity, and bioavailability of drugs[3] and prevent the first-pass metabolism of the drug molecules through a lymphatic uptake mechanism.[4] Additionally, nanoparticles are particularly useful for cancer chemoprevention for their enhanced permeability and retention effect.[5] Therefore, significant efforts in recent years have been devoted to the fabrication and use of nanoparticles for targeted drug delivery and targeted cancer therapy.[6]

Molecular self-assembly is the spontaneous organization of molecules due to their mutual interaction (from the noncovalent type) into ordered aggregates (spatial and/or temporal ordering) without external control,[7–9] and it is an elegant and powerful approach to the design of nanomaterials.[10] In recent years, self-assembly between proteins and polysaccharides has gained great interest in the fabrication of nanoparticles for delivering drugs and bioactive molecules.[11] One of the most common methods for the self-assembly of proteins and polysaccharides into particles is the mixing of oppositely charged polyelectrolytes under appropriate solution conditions.[12,13]

Chitosan (CS), a well-known natural polysaccharide composed of glucosamine and *N*-acteyl glucosamine units via β-(1→4) linkages, can dissolve in an acidic solution and become the only cationic polysaccharide because of the protonation of amino groups on its backbone.[14] CS has received significant interest in medical and pharmaceutical applications because of its biodegradability, biocompatibility, and safety in both animal models[15] and humans.[16] Soy protein is an abundant, renewable, and inexpensive natural protein; it has gained considerable attention

for its potential roles in improving risk factors for cardiovascular disease.[17] β-conglycinin (7S) is one of the two major globulins of soy protein, and its isoelectric point (pI) is approximately 4.8. 7S possess a net negative charge above its pI, whereas CS has a net positive charge in acid solution. So, they can generate nanoparticles through electrostatic interactions.

5-Fluorouracil (5-FU), an antineoplastic agent, is widely used for the treatment of various types of solid tumors. It has a short biological half-life because of its rapid metabolism, incomplete and nonuniform oral absorption,[18] and serious side effects because of its nonselective action against healthy cells.[18,19] To improve the short biological half-life and reduce its side effects, the incorporation of 5-FU into nanocarriers for delivery is one of the most effective strategies.[20]

In this study, nanoparticles based on 7S and CS were fabricated with the self-assembly method. Turbidity measurements were used to investigate the effect of the pH, 7S-to-CS mass ratio, and total concentration of 7S and CS on the formation of the nanoparticles. The structure and properties of the nanoparticles were studied by Fourier transform infrared (FTIR) spectroscopy, scanning electron microscopy (SEM), and dynamic light scattering (DLS), and the release behaviors and release mechanism of 5-FU from the nanoparticles were also investigated in detail.

EXPERIMENTAL

Materials and Chemicals

7S (protein content = 90.16%) was prepared according to Nagano *et al.*[21] CS (deacetylation degree > 95%), glutaraldehyde (GA, 50% solution), and 5-FU (99%) were purchased from Aladdin (Shanghai, China). The other reagents were analytical grade and were used as received.

Self-Assembly of Blank Nanoparticles Composed of 7S and CS

A certain concentration of 7S solution was prepared by the dispersion of the 7S powder in an aqueous solution with a pH of 10 to completely dissolution with magnetic stirring, whereas a certain concentration of CS solution was prepared by the dispersion of the CS powder in 1% v/v acetic acid solution with magnetic stirring. Under constant magnetic stirring, the 7S solution was added dropwise into the CS solution with a syringe, and the mixture was kept stirring for 30 min. Through the variation of the 7S-to-CS mass ratio and the total concentration of 7S and CS and the adjustment of the pH of the mixture with 2 mol/L HCl or NaOH solution, the effects of the mass ratio, total concentration, and pH on the self-assembly of the nanoparticles were investigated according to the turbidity method described in the literature.[22–24]

The turbidity was measured according to the literature[22–24] but with some modifications. Briefly, after the mixture was left for 10 min, the mixture was gently poured into a 1-cm cuvette, and the turbidity was then rapidly determined at 600 nm in a ultraviolet–visible (UV–vis) spectrophotometer (UVmini-1240, Shimadzu, Japan).

Self-Assembly of 5-FU-Loaded Nanoparticles Composed of 7S and CS

As described in the previous section, the 7S solution with 5-FU was added dropwise into the CS solution with a syringe, and the mixture was stirred for 30 min. Then, glutaraldehyde [30 μg/mg (7S and CS)] was added to crosslink amino groups along the 7S and CS backbones overnight under constant magnetic stirring to obtain stable nanoparticles. Excess glutaraldehyde was neutralized with sodium bisulfite. Finally, the mixture was centrifuged at 15,000 g for 30 min, and the precipitate was freeze-dried for 24 h by a freeze dryer (LL3000, Heto, Germany) to obtain the 5-FU-loaded nanoparticles.

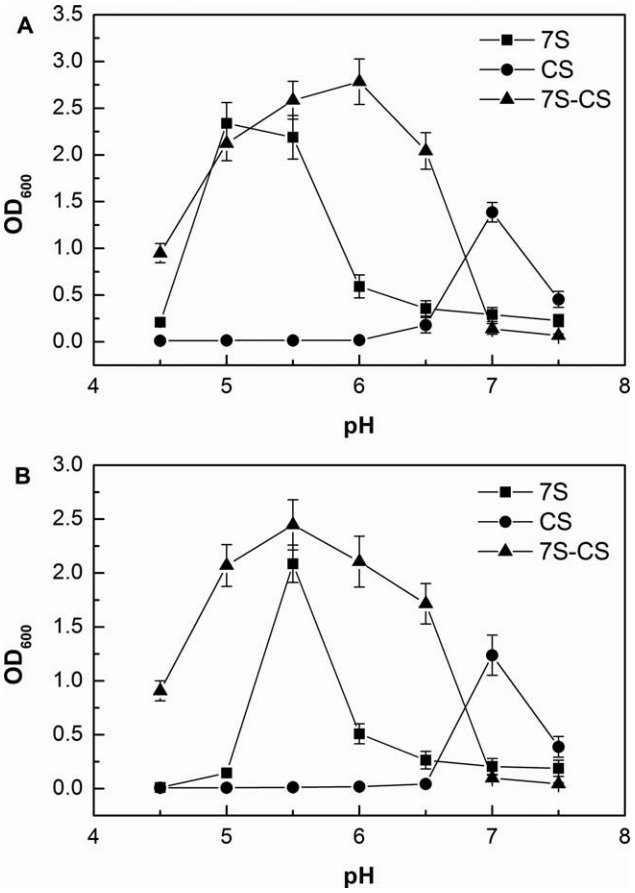

Figure 1. Turbidity profiles as a function of pH for measurements at (A) 10 min and (B) 24 h with a total concentration of 0.9 mg/mL and a 7S-to-CS mass ratio of 2 : 1. OD_{600} = optical dense obtained at 600 nm.

To determine the encapsulation efficiency (EE) and loading efficiency (LE) of 5-FU, the 5-FU in the supernatant was determined by the UV–vis spectrophotometer according to the established standard curve, whereas the dried 5-FU-loaded nanoparticles were weighed accurately. The EE and LE values of the samples were calculated with the following equations:

$$\mathrm{EE}(\%) = \frac{\text{Total 5-FU} - \text{Free 5-FU}}{\text{Total 5-FU}} \times 100 \quad (1)$$

$$\mathrm{LE}(\%) = \frac{\text{Total 5-FU} - \text{Free 5-FU}}{\text{Nanoparticle Weight}} \times 100 \quad (2)$$

FTIR Spectroscopy Study

Each dried sample ground with KBr was compressed into a tablet, and then, the spectrum was recorded by an FTIR

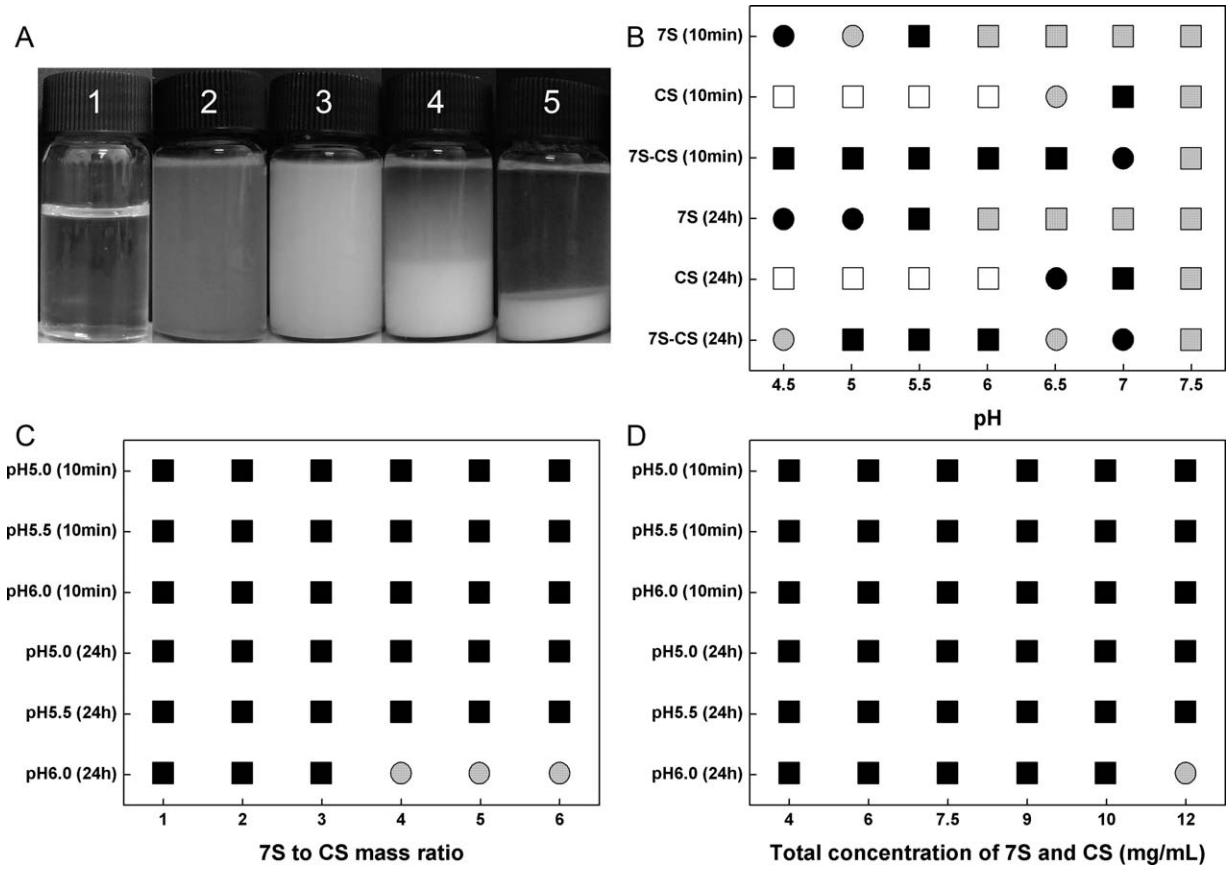

Figure 2. (A) Phase diagram and effects of (B) pH (mass ratio = 4 : 1, total concentration = 9 mg/mL), (C) 7S-to-CS mass ratio (pH = 5.5, total concentration = 9 mg/mL), and (D) total concentration of 7S and CS (pH = 5.5, mass ratio = 4 : 1): (□) transparent, (■) translucent, (■) turbid, (●) partly phase separation, and (●) totally phase separation.

spectroscope (Nexus 670, Nicolet) with an average of 16 scans from 4000 to 500 cm^{-1} at a resolution of 0.2 cm^{-1}.

Surface Morphological Analysis

SEM was performed to examine the surface morphologies of the nanoparticles. The freeze-dried nanoparticles were first sputter-coated with conductive carbon, and then, the morphology was examined with SEM (Supra 55, Zeiss, Germany) with an acceleration voltage of 20 kV.

Particle Size Measurement

The particle size and size distribution of the nanoparticles were performed by DLS with a particle size analyzer (ZS90, Malvern).

In Vitro Drug-Release Study

The 5-FU-loaded nanoparticles were put into a dialysis bag, and the dialysis bag was clamped by a clip. Then, the dialysis bag containing 5-FU-loaded nanoparticles was immersed in a conical vial containing 60 mL of buffer solution. The vial was closed and incubated in a thermostatic shaker (SKY100C, Sukun, China) at a speed of 60 rpm at 37°C. At given time intervals, 3 mL of the solution was taken out to measure the amount of 5-FU release with a UV–vis spectrophotometer at 265 nm, and 3 mL of fresh buffer solution was put back into the same vial. The amount of 5-FU release was obtained from the standard curve. The cumulative release of 5-FU was calculated with the following equation:

$$\text{Cumulative release of } 5\text{-FU}(\%) = \frac{M_t}{M_o} \times 100 \quad (3)$$

where M_t is the cumulative amount of 5-FU released at time t and M_0 is the initial amount of 5-FU loaded.

RESULTS AND DISCUSSION

Effect of pH on the Turbidity

Turbidity measurement, a fast and practical method, has been widely used for monitoring complex coacervation or aggregation processes in various protein–polysaccharides systems[25–30] because the variations of absorbance will reveal the appearance of coacervates or aggregates through modification of the light properties of the systems.[31] An increase in the turbidity values is primarily due to an increase in the particle number and size,[31,32] whereas a decrease in the turbidity values is mainly due to large-scale aggregation and the subsequent precipitation of biopolymers.[30]

The turbidity measurement (Figure 1) and phase diagram [Figure 2(B)] as a function of pH was used to study the effect of pH on the self-assembly of 7S and CS. The turbidity of the 7S solution [Figure 1(A)] increased rapidly between pH 4.5 and 5.0 with a peak at pH 5.0 and subsequently decreased at more alkaline pHs; this was consistent with the phase behavior of translucent, turbid, partial and total phase separation

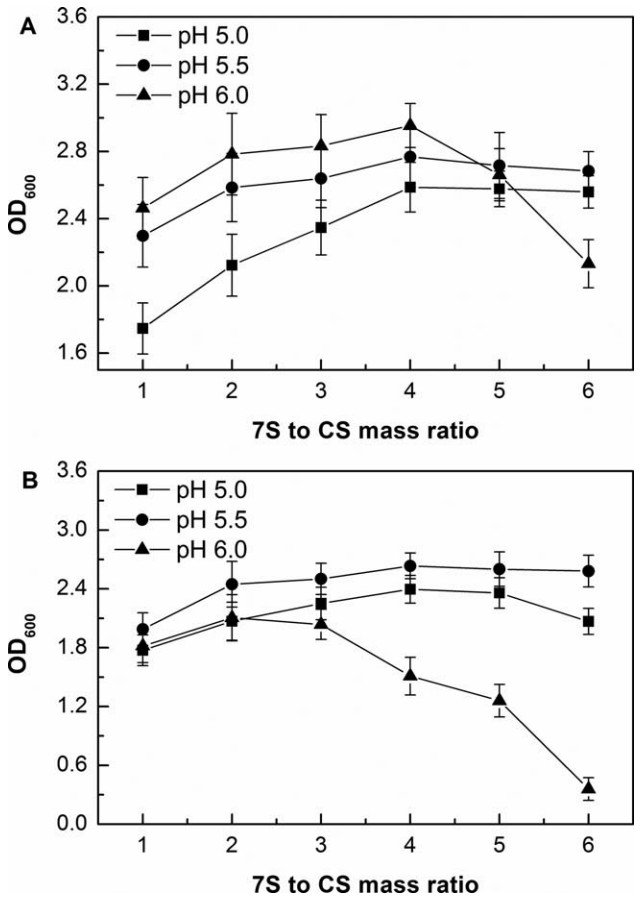

Figure 3. Turbidity profiles as a function of the 7S-to-CS mass ratio for measurements at (A) 10 min and (B) 24 h with a total concentration of 0.9 mg/mL.

[Figure 2(B)]. The increase in the turbidity was due to increases in the number and size and a decrease in the solubility of the 7S aggregates, whereas the decrease in the turbidity was due to the decrease in the number and size and increase in the solubility of 7S aggregates. The maximum turbidity of the 7S solution at pH 5.0 was considered to be due the reduction in the electrostatic repulsion between 7S molecules around their pI (4.8) and the size and number of particles. The turbidity of the CS solution [Figure 1(A)] was transparent from pH 4.5 to 6.0, but the turbidity began to increase above pH 6.0, peaked at pH 7.0, and subsequently decreased to a low value; this was is in accordance with the phase behavior of the transparent, translucent, turbid, and partial phase separation [Figure 2(B)]. The maximum turbidity of the CS solution at pH 7.0 was primarily related to the deprotonation of amine groups along the CS backbone; this resulted in self-association at the dislocation constant of CS ($pK_a = 7.0$) and the subsequent insolubility of CS. The turbidity curve of the 7S–CS solution [Figure 1(A)] was significantly different from that of 7S and CS independently; this indicated that there were interactions between 7S and CS. The turbidity of the 7S–CS solution increased from pH 4.5 to 6.0, peaked at pH 6.0, and subsequently decreased as the pH became more alkaline; this was in agreement with the phase behavior [Figure 2(B)]. The pH of the medium strongly influenced the charge density of the proteins and polysaccharides and, consequently, their interaction. 7S carried negative charges only at pHs above its pI, whereas CS carried positive charges only at pHs below its pK_a. The coacervation between 7S and CS occurred in the pH range 5.0–6.5 because of electrostatic interaction between oppositely charged groups. The increase in the turbidity was due to the increase of the number and size of coacervates, and the maximum turbidity at pH 6.0 was due to the maximum number of coacervates. Subsequently, the decrease in turbidity was due to the large-scale aggregation and the subsequent precipitation of coacervates.

To obtain more insight into the interaction between 7S and CS, the turbidity of the 7S–CS mixture left for 24 h was measured [Figure 1(B)]. As illustrated in Figure 1(B), the maximum turbidity of 7S, CS, and 7S–CS was at pH 5.5, 7.0, and 5.5, respectively. Compared with Figure 1(A), the maximum turbidity of 7S–CS was moved from 6.0 to 5.5, and the 7S–CS mixture showed good stability at pH 5.5 because 7S–CS association was the result of the balance effect of various attractive forces (e.g., van der Waal's, hydrophobic, and electrostatic interaction between oppositely charged groups) and various repulsive forces (e.g., electrostatic interaction between similarly charged groups).[33] These turbidity variations were consistent with the phase behavior [Figure 2(B)].

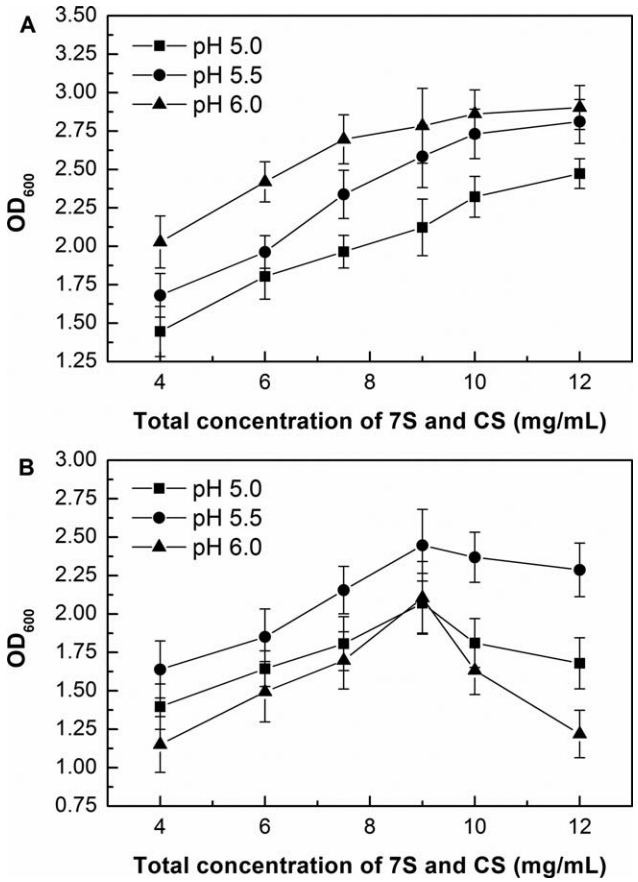

Figure 4. Turbidity profiles as a function of the total concentration for measurements at (A) 10 min and (B) 24 h with a 7S-to-CS mass ratio of 2 : 1.

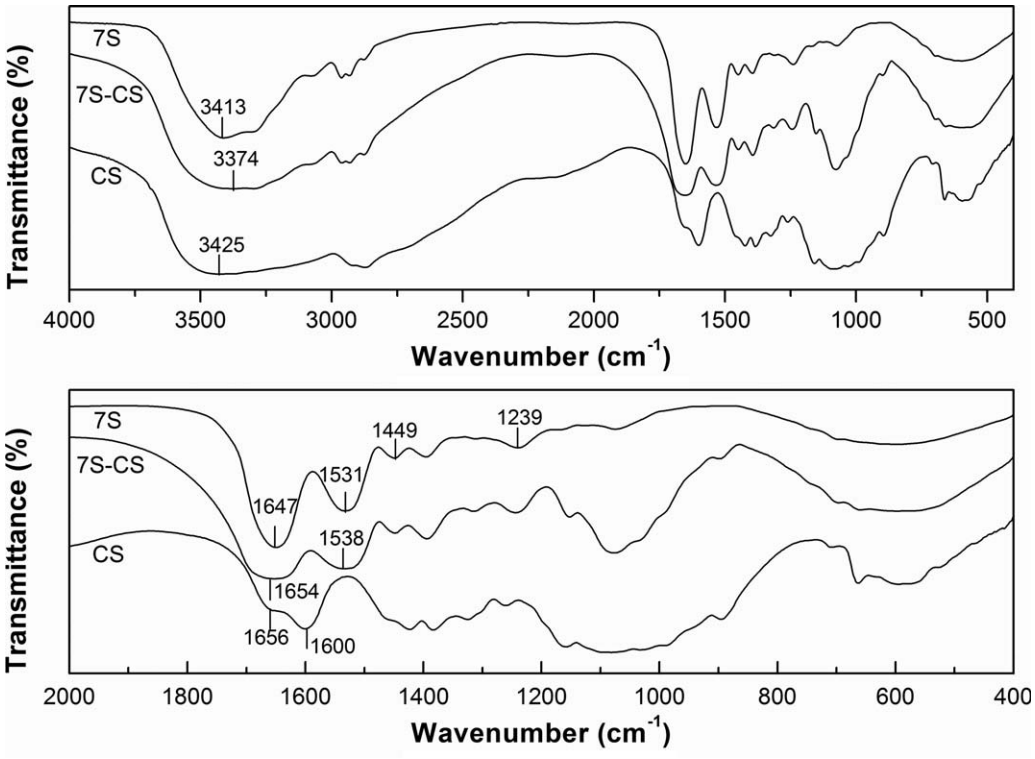

Figure 5. FTIR spectra of 7S, CS, and 7S–CS nanoparticles.

Effect of the 7S-to-CS Mass Ratio on the Turbidity

The biopolymer mixing ratio is a critical parameter for controlling the balance of biopolymer charge and the intensity of the electrostatic interaction,[31,34] and consequently, it has major effects on the turbidity and degree of sediment formation in the mixed solution. The turbidity and phase diagram as a function of the 7S-to-CS mass ratio were measured and are shown in Figures 2(C) and 3, respectively. The turbidity increased with the 7S-to-CS mass ratio and then decreased after the maximum at a 7S-to-CS mass ratio of 4 : 1 [Figure 3(A)]. With the increase in the 7S-to-CS mass ratio, more protein molecules with negative charges were available per CS chain. This influenced the charge balance and interaction intensity between 7S and CS. When the mass ratio exceeded 4 : 1, the complex particles were larger and more unstable, and this resulted in sediment formation and, consequently, low turbidity. The mixture at pH 5.5 showed the maximum turbidity and the best stability [Figure 3(B)] because of the formation of small and stable particles. The phase behavior [Figure 2(C)] confirmed the results of the turbidity variations.

Effect of the Total Concentration of 7S and CS on the Turbidity

The effects of the total concentration on the turbidity and phase diagram of the 7S and CS mixtures are shown in Figures 2(D) and 4. The turbidity of the mixture increased with the increase in the total concentration of 7S and CS [Figure 4(A)]. The turbidity of the mixture left for 24 h decreased after the maximum at total concentration of 9 mg/mL, and the maximum was at a pH of 5.5 [Figure 4(B)]. The total concentration of biopolymer is an important parameter for controlling the particle number and stability of a mixture. When the total concentration increases, the particle number increases, and consequently, the interaction between particles to form large and unstable particles increases. This results in a decrease in the turbidity. The phase behavior in this study [Figure 2(D)] also confirmed the results of the turbidity variations.

According to the analyses for the influence of pH, mass ratio, and total concentration on the turbidity above, a pH of 5.5, mass ratio of 4 : 1, and total concentration of 9 mg/mL were chosen for preparing the nanoparticles.

FTIR Analysis

The FTIR spectra of 7S, CS, and 7S–CS are shown in Figure 5. The FTIR spectrum of 7S showed main characteristic bands at 3413 cm^{-1} concerned with O—H stretching vibrations, 1647 cm^{-1} attributed to C═O stretching (amide I), 1531 cm^{-1} assigned to N—H bending (amide II), 1449 cm^{-1} corresponding to symmetric COO^-, and 1239 cm^{-1} associated with C—H vibrations in peptide bonds (amide III).[35] The FTIR spectrum of CS showed the main characteristic band at 3425 cm^{-1} assigned to O—H stretching vibrations. Other characteristic bands were also observed at 1656 cm^{-1} attributed to amide I (C═O) and 1600 cm^{-1} assigned to amide III ($—NH_3^+$ groups).[36] The FTIR spectrum of the 7S–CS coacervates displayed characteristic bands at 3374 cm^{-1} concerned with O—H stretching vibrations and 1654 and 1538 cm^{-1} attributed to the stretching vibrations of $—COO^-$ and $—NH_3^+$ groups, respectively. In comparison with the FTIR spectra of 7S and CS, the FTIR of 7S–CS changed significantly in the carbonyl–amide region: the band at 1654 cm^{-1} for 7S–CS was much broader than those for 7S and CS; the $—NH_3^+$ groups (band at 1600 cm^{-1}) and

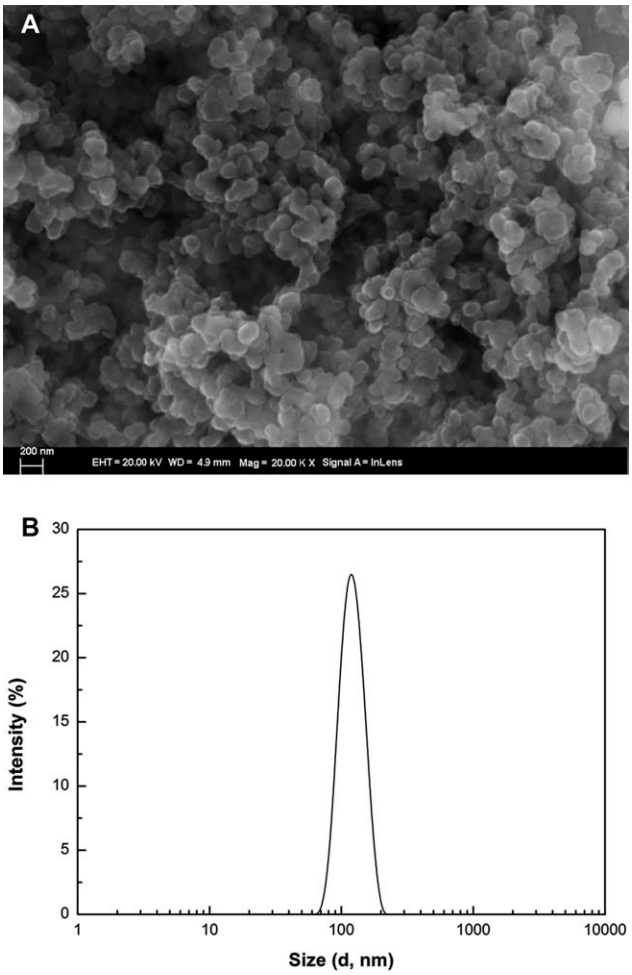

Figure 6. (A) SEM micrograph and (B) particle size distribution of nanoparticles. The nanoparticles were obtained under the following conditions: pH = 5.5, mass ratio = 4 : 1, total concentration = 9 mg/mL, and 5-FU concentration = 1 mg/mL.

asymmetric and symmetric —COO^- stretching vibrations at 1647 and 1531 cm^{-1}, respectively, disappeared. These changes indicated the presence of the electrostatic interaction between the amine groups of CS (—NH_3^+) and the carboxyl groups of 7S (—COO^-).[36,37] Additionally, compared with 7S (band at 3413 cm^{-1}) and CS (band at 3425 cm^{-1}), the O—H stretching vibration band of 7S–CS shifted to a low wave number (band at 3374 cm^{-1}); this indicated that intermolecular hydrogen bonds were also involved in the nanoparticles.[38]

Morphological Analysis and Size Distribution

The morphology of the 5-FU-loaded nanoparticles was investigated with SEM [Figure 6(A)]. The nanoparticles had a spherical or approximately spherical morphology with a smooth surface, and the size of the nanoparticles observed from SEM was in the range of 70–140 nm. The mean size was about 90 nm. The size distribution of the 5-FU-loaded nanoparticles was also calculated by DLS measurement [Figure 6(B)]. The mean size of the nanoparticles observed from DLS was found to be about 120 nm, with a polydispersity index of 0.265. The low polydispersity index clearly indicated a narrow size distribution of the prepared nanoparticles. Compared with the particle size observed from SEM and DLS, the particle size obtained from SEM was 25% lower than those measured with DLS. This difference was due to the fact that DLS measured the particle size in solution, whereas SEM analyzed the particle size in a freeze-dried state, which caused the shrinkage of nanoparticles by the cast-drying process in the vacuum environment.[39–41]

In Vitro Drug Release

The EE and LE values were 68.57 and 16.92%, respectively. The kinetic release profiles of 5-FU at different pHs at 37°C are shown in Figure 7. The release of 5-FU from the nanoparticles showed two distinct release behaviors; it started with an initial burst release and was followed by a sustained release. In the first 60 min, the initial burst release was observed, and 40.67 and 48.14% of 5-FU were released at pHs of 1.2 and 7.4, respectively. After 60 min, the sustained release was also observed, in which the cumulative release of 5-FU increased slowly with time and, at the end of 600 min, reached 67.42 and 93.45% at pHs of 1.2 and 7.4, respectively. The phenomenon of burst release effect was due to the release of 5-FU, which was associated with the surface of the nanoparticles and those that were interacting weakly with the nanoparticles. The subsequent sustained release was attributed to the release of 5-FU that were incorporated more deeply into the nanoparticles; this resulted in a longer distance for 5-FU release. In addition, the percentages of 5-FU release mentioned previously indicated that the release behavior of 5-FU was pH-dependent. When the pH (1.2) was below the pI of 7S and the pK_a of CS, the carboxyl anion groups along the 7S backbone became carboxyl acid groups by the protonation and, thus, formed hydrogen bonds with the polar groups in the nanoparticles. This resulted in a more compact network structure in the nanoparticles, whereas the protonation of amine groups along the CS backbone resulted in a more expanding network structure because of the charge repulsive forces. However, the hydrogen bonds were dominant because the mass of 7S was four times that of CS; this resulted in a lower release at pH 1.2. When the pH (7.4) was above the pI of

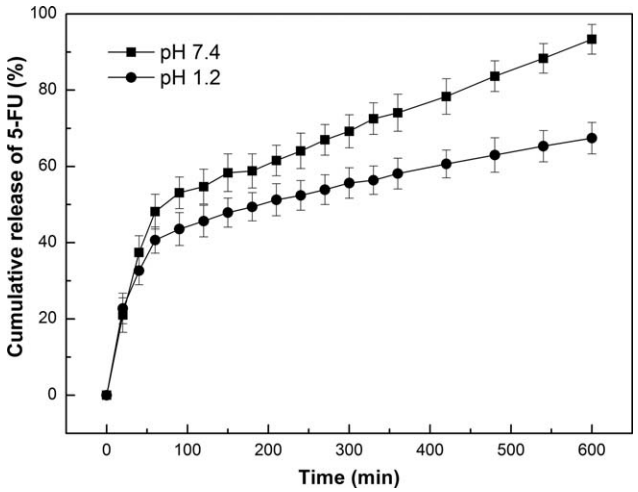

Figure 7. Profiles of 5-FU release from the nanoparticles as a function of time. pHs of 1.2 and 7.4 were used to simulate the release environment of the stomach and the small intestine, respectively.

7S and the pK_a of CS, the deprotonation of carboxyl acid groups caused electrostatic repulsion and, consequently, resulted in a more expanding network structure, whereas the deprotonation of amine groups also produced hydrogen bonds, which led to a compact network structure. As a result, the electrostatic repulsion was dominant for the 7S-to-CS mass ratio of 4 : 1, and this led to a higher release pH of 7.4.

To investigate the release mechanism of 5-FU from the nanoparticles, we analyzed the release data by fitting them to the following equation:[42,43]

$$\frac{M_t}{M_\infty} = kt^n \quad (4)$$

where M_t/M_∞ is the fractional release of 5-FU at time t, k is the release constant, and n is the characteristic exponent related to the release mechanism of 5-FU. For spherical systems, $n \leq 0.43$, $0.43 < n < 0.85$, $n = 0.85$, and $n > 0.85$ are the values for the release mechanisms of Fickian diffusion, anomalous (non-Fickian) transport, case II transport (zero-order diffusion), and super case II transport, respectively. $M_t/M_\infty \leq 0.6$ should only be used in this equation.

The values of n obtained from the slope of the plot of $\ln(M_t/M_\infty)$ versus $\ln t$ for 5-FU release at pH 1.2 and 7.4 were 0.29 ($R^2 = 0.97019$) and 0.42 ($R^2 = 0.94982$), respectively. These results indicate that the release mechanism of 5-FU was Fickian diffusion, and the diffusion rate of 5-FU at pH 1.2 was lower than that at pH 7.4; this was consistent with the results in Figure 7.

CONCLUSIONS

The nanoparticles were fabricated with a self-assembly method between 7S and CS. The turbidity measurement was used to investigate the effect of the pH, 7S-to-CS mass ratio, and total concentration of 7S and CS on the formation of the nanoparticles, and the FTIR, SEM, and DLS were also used to study the structures and properties of the nanoparticles. The optimum conditions for preparing nanoparticles were a pH of 5.5, a 7S-to-CS mass ratio of 4 : 1, and a total concentration of 7S and CS of 9 mg/mL. The nanoparticles were formed through electrostatic interactions between the amine groups of CS ($-NH_3^+$), the carboxyl groups of 7S ($-COO^-$), and intermolecular hydrogen bonds. The nanoparticles were approximately spherical, with a mean particle size of 120 nm. 5-FU from the nanoparticles released slowly after the initial burst release, and its release was pH-dependent. The release mechanism of 5-FU was Fickian diffusion according to the Ritger–Peppas model.

ACKNOWLEDGMENTS

This work was financially supported by the Natural Science Foundation of Guangdong Province (contract grant number s2012040007710) and the Natural Science Foundation of Zhaoqing University (contract grant number 201201).

REFERENCES

1. Chomoucka, J.; Drbohlavova, J.; Huska, D.; Adam, V.; Kizek, R.; Hubalek, J. *Pharmacol. Res.* **2010**, *62*, 144.
2. Yu, S.; Hu, J.; Pan, X.; Yao, P.; Jiang, M. *Langmuir* **2006**, *22*, 2754.
3. Roger, E.; Lagarce, F.; Garcion, E.; Benoit, J. P. *Nanomedicine* **2010**, *5*, 287.
4. Grama, C. N.; Ankola, D. D.; Kumar, M. N. V. R. *Curr. Opin. Colloid Interface Sci.* **2011**, *16*, 238.
5. Siddiqui, I. A.; Adhami, V. M.; Bharali, D. J.; Hafeez, B. B.; Asim, M.; Khwaja, S. I.; Ahmad, N.; Cui, H.; Mousa, S. A.; Mukhtar, H. *Cancer Res.* **2009**, *69*, 1712.
6. Brannon-Peppas, L.; Blanchette, J. O. *Adv. Drug Delivery Rev.* **2012**, *64*, 206.
7. Mendes, A. C.; Baran, E. T.; Reis, R. L.; Azevedo, H. S. *Wiley Interdiscip. Rev. Nanomed. Nanobiotechnol.* **2013**, *5*, 582.
8. Whitesides, G. M.; Grzybowski, B. *Science* **2002**, *295*, 2418.
9. Whitesides, G. M.; Mathias, J. P.; Seto, C. T. *Science* **1991**, *254*, 1312.
10. King, N. P.; Sheffler, W.; Sawaya, M. R.; Vollmar, B. S.; Sumida, J. P.; André, I.; Gonen, T.; Yeates, T. O.; Baker, D. *Science* **2012**, *336*, 1171.
11. Jones, O. G.; McClements, D. *J. Adv. Colloid Interfaces* **2011**, *167*, 49.
12. Ron, N.; Zimet, P.; Bargarum, J.; Livney, Y. D. *Int. Dairy J.* **2010**, *20*, 686.
13. Jones, O.; Decker, E. A.; McClements, D. *J. Food Hydrocolloids* **2010**, *24*, 239.
14. Luo, Y.; Wang, Q. *Int. J. Biol. Macromol.* **2014**, *64*, 353.
15. Roy, K.; Mao, H. Q.; Huang, S. K.; Leong, K. W. *Nat. Med.* **1999**, *5*, 387.
16. Maezaki, Y.; Tsuji, K.; Nakagawa, Y.; Kawai, Y.; Akimoto, M.; Tsugita, T.; Takekawa, W.; Terada, A.; Hara, H.; Mitsuoka, T. *Biosci. Biotechnol. Biochem.* **1993**, *57*, 1439.
17. Gupta, S. S.; Ghosh, M. *J. Food Eng.* **2014**, *121*, 64.
18. Rejinold, N. S.; Muthunarayanan, M.; Chennazhi, K. P.; Nair, S. V.; Jayakumar, R. *Int. J. Biol. Macromol.* **2011**, *48*, 98.
19. Wilson, B.; Ambika, T. V.; Patel, R. D. K.; Jenita, J. L.; Priyadarshini, S. R. B. *Int. J. Biol. Macromol.* **2012**, *51*, 874.
20. Li, S.; Wang, A.; Jiang, W.; Guan, Z. *BMC Cancer* **2008**, *8*, 103.
21. Nagano, T.; Hirotsuka, M.; Mori, H.; Kohyama, K.; Nishinari, K. *J. Agric. Food Chem.* **1992**, *40*, 941.
22. Bachar, M.; Mandelbaum, A.; Portnaya, I.; Perlstein, H.; Even-Chen, S.; Barenholz, Y.; Danino, D. *J. Controlled Release* **2012**, *160*, 164.
23. Tsai, S. W.; Liu, R. L.; Hsu, F. Y.; Chen, C. C. *Biopolymers* **2006**, *83*, 381.
24. Silva, M. C.; Andrade, C. T.; Alimentos, P. C. D.; Química, I. D. *Polimeros* **2009**, *19*, 133.
25. Stone, A. K.; Nickerson, M. T. *Food Hydrocolloids* **2012**, *27*, 271.
26. Singh, S. S.; Siddhanta, A. K.; Meena, R.; Prasad, K.; Bandyopadhyay, S.; Bohidar, H. B. *Int. J. Biol. Macromol.* **2007**, *41*, 185.
27. Weinbreck, F.; Nieuwenhuijse, H.; Robijn, G. W.; de-Kruif, C. G. *Langmuir* **2003**, *19*, 9404.

28. Lee, A. C.; Hong, Y. H. *Food Res. Int.* **2009**, *42*, 733.
29. Pedersen, H. C. A.; Jørgensen, B. B. *Food Hydrocolloids* **1991**, *5*, 323.
30. Gorji, S. G.; Gorji, E. G.; Mohammadifar, M. A. *Food Hydrocolloids* **2014**, *34*, 161.
31. Schmitt, C.; Sanchez, C.; Thomas, F.; Hardy, J. *Food Hydrocolloids* **1999**, *13*, 483.
32. Yuan, Y.; Wan, Z. L.; Yang, X. Q.; Yin, S. W. *Food Res. Int.* **2014**, *55*, 207.
33. Hosseini, S. M. H.; Emam-Djomeh, Z.; Razavi, S. H.; Moosavi-Movahedi, A. A.; Saboury, A. A.; Atri, M. S.; Meeren, P. V. D. *Food Hydrocolloids* **2013**, *32*, 235.
34. Ye, A. *Int. J. Food Sci. Technol.* **2008**, *43*, 406.
35. Teng, Z.; Luo, Y.; Wang, Q. *J. Agric. Food Chem.* **2012**, *60*, 2712.
36. Espinosa-Andrews, H.; Sandoval-Castilla, O.; Vázquez-Torres, H.; Vernon-Carter, E. J.; Lobato-Calleros, C. *Carbohydr. Polym.* **2010**, *79*, 541.
37. Shi, X.; Du, Y.; Sun, L.; Zhang, B.; Dou, A. *J. Appl. Polym. Sci.* **2006**, *100*, 4614.
38. Liu, Y.; Cui, Y.; Liao, M. *J. Appl. Polym. Sci.* **2014**, *131*, 1.
39. Zou, T.; Li, S. L.; Zhang, X. Z.; Wu, X. J.; Cheng, S. X.; Zhuo, R. X. *J. Polym. Sci. Part A: Polym. Chem.* **2007**, *45*, 5256.
40. Mirshahi, T.; Irache, J. M.; Gueguen, J.; Orecchioni, A. M. *Drug Dev. Ind. Pharm.* **1996**, *22*, 841.
41. Li, Z.; Percival, S. S.; Bonard, S.; Gu, L. *Mol. Nutr. Food Res.* **2011**, *55*, 1096.
42. Domaratzki, R. E.; Ghanem, A. *J. Appl. Polym. Sci.* **2013**, *128*, 2173.
43. Liu, Y.; Cui, Y. *J. Appl. Polym. Sci.* **2011**, *120*, 3613.